arXiv:cond-mat/0604596v1 [cond-mat.mtrl-sci] 26 Apr 2006

Importance of second-order piezoelectric effects in zincblende semiconductors

Gabriel Bester,[1] Xifan Wu,[2] David Vanderbilt,[2] and Alex Zunger[1]

[1]*National Renewable Energy Laboratory, Golden, Colorado 80401*

[2]*Department of Physics and Astronomy, Rutgers University, Piscataway, New Jersey 08854, USA*

(Dated: January 2, 2022)

We show that the piezoelectric effect that describes the emergence of an electric field in response to a crystal deformation in III-V semiconductors such as GaAs and InAs has strong contributions from second-order effects that have been neglected so far. We calculate the second-order piezoelectric tensors using density functional theory and obtain the piezoelectric field for [111]-oriented $In_xGa_{1-x}As$ quantum wells of realistic dimensions and concentration x. We find that the linear and the quadratic piezoelectric coefficients have the opposite effect on the field, and for large strains the quadratic terms even dominate. Thus, the piezoelectric field turns out to be a rare example of a physical quantity for which the first- and second-order contributions are of comparable magnitude.

PACS numbers: 77.65.-j,77.65.Bn,77.65.Ly,78.67.De,71.15.-m

Since the discovery of piezoelectricity in 1880 by the Curie brothers [1], widespread efforts have been aimed at understanding this peculiar effect and developing its applications. Piezoelectric materials are in use today in a wide range of devices, including ultrasonic transducers for medical and sonar imaging and various types of micropositioners and actuators. Since the early days, the effect has been understood as arising from displacement of the ions in response to a mechanical deformation, leading to the appearance of charges on some of the crystal's surfaces [1]. Despite some early doubts, it is now well established [2, 3, 4, 5, 6] that this is a *bulk* effect. It has two components; the contribution coming from the ionic displacements tends to be compensated by the purely electronic (frozen-ion) response, resulting in a subtle balance between ionic and electronic contributions [3, 4, 5].

Until now, theoretical modeling of the piezoelectric effect in bulk solids [7], quantum wells (Ref. 8 and references therein) and more recently in quantum dots [9, 10, 11, 12, 13, 14] has focused exclusively on the first-order piezoelectric tensor $\tilde{e}_{\mu j}$, neglecting possible higher-order terms. That is, if $P_\mu = \sum_j e_{\mu j}\eta_j + \frac{1}{2}\sum_{jk} B_{\mu jk}\eta_j\eta_k + ...$, where P is the polarization and η is the strain, previous work has concentrated on the linear coefficient $e_{\mu j}$ to the exclusion of the quadratic coefficient $B_{\mu jk}$.

Recent experimental determinations of piezoelectric constants (e.g., Refs. 15, 16, 17, 18, 19, 20, 21) have tended to follow this approach, interpreting the measured piezoelectric fields by assuming a linear relationship between polarization and strain (retaining $e_{\mu j}$ but neglecting $B_{\mu jk}$). Indeed, the experimental procedures used thus far to deduce piezoelectric constants from measured fields have made it easy to overlook the importance of the second-order piezoelectric effect, because measurements were restricted to heterostructure quantum wells with small lattice mismatch (those with large lattice mismatch, like high-In-content (In,Ga)As/GaAs structures, were avoided because they tend to develop unwanted dislocations). Similarly, experiments for quantum wells or bulk materials under pressure have tended to probe only a very small region of strain, so that a clear signature of the quadratic dependence of field upon strain is difficult to detect.

In this Letter we show, using self-consistent density-functional theory (DFT) calculations for GaAs and InAs, that the hitherto neglected second-order piezoelectric tensor gives significant contributions to the piezoelectric field. We show that neglecting the second-order piezoelectric tensor leads to an overestimation by 200% in the piezoelectric field for $In_xGa_{1-x}As$ quantum wells on GaAs in the experimentally accessible range of concentration x. For higher In concentrations, accessible in quantum dots, second-order terms will dominate over first-order terms. This new insight is important because it represents a paradigm shift in the interpretation of measurements of piezoelectricity in quantum wells and quantum dots.

We find it most convenient to formulate the piezoelectric response in terms of the *reduced* (and dimensionless) polarization p_μ defined implicitly via $P_\alpha = \frac{e}{\Omega}\sum_\mu p_\mu a_\alpha^{(\mu)}$, where e is the charge quantum, Ω is the cell volume, P_α is the polarization in Cartesian coordinates, and $a_\alpha^{(\mu)}$ is the α'th component of the μ'th strain-deformed lattice vector. We expand this reduced polarization, retaining the *second-order* strain as

$$p_\mu = \sum_j \tilde{e}^0_{\mu j}\ \eta_j + \frac{1}{2}\sum_{jk} \widetilde{B}_{\mu jk}\ \eta_j\eta_k \quad . \tag{1}$$

The reduced proper piezoelectric tensor is then

$$\tilde{e}_{\mu j} = \frac{dp_\mu}{d\eta_j} = \tilde{e}^0_{\mu j} + \sum_k \widetilde{B}_{\mu jk}\,\eta_k \quad , \tag{2}$$

where we use η_j (j=1,6) to denote strain in the Voigt notation. Here $\tilde{e}^0_{\mu j}$ is the reduced proper piezoelectric tensor of the unstrained material, while $\widetilde{B}_{\mu jk}$ is a fifth rank tensor with Cartesian coordinates μ and the strain index in Voigt notation j, k and represents the first-order

TABLE I: Linear and quadratic piezoelectric coefficients (C/m^2) as calculated from DFT.

	e_{14}	B_{114}	B_{124}	B_{156}
InAs	−0.115	−0.531	−4.076	−0.120
GaAs	−0.230	−0.439	−3.765	−0.492

change of the reduced piezoelectric tensor with strain. We obtain $\tilde{e}^0_{\mu j}$ and $\widetilde{B}_{\mu jk}$ from first-principles calculations in a manner described next.

First-principles calculation of linear and non-linear piezoelectric coefficients: Symmetry considerations for the zincblende crystal structure imply that the only nonzero elements of the piezoelectric tensor are $\tilde{e}^0_{14} = \tilde{e}^0_{26} = \tilde{e}^0_{36}$ (i.e., there is only one independent element). Similar considerations guarantee that there are only 24 non-zero elements of the $\widetilde{B}_{\mu jk}$ tensor, which can be reduced to three independent elements $\widetilde{B}_{114}$, $\widetilde{B}_{124}$, and $\widetilde{B}_{156}$. (The other nonzero elements are obtained by applying cyclic permutations $x \to y \to z$ or interchanges such as $x \leftrightarrow y$ on the Cartesian axes, e.g., $\widetilde{B}_{114} = \widetilde{B}_{225}$, $\widetilde{B}_{124} = \widetilde{B}_{235} = \widetilde{B}_{215}$, and $\widetilde{B}_{156} = \widetilde{B}_{225}$.) We carried out *ab-initio* calculations of these tensor elements using a plane-wave pseudopotential approach to DFT in the local-density approximation (LDA) as implemented in the ABINIT code package[22]. First, we relaxed the lattice parameters for both GaAs and InAs. Next, linear-response calculations of the linear bulk piezoelectricconstant $\tilde{e}^0_{14}$ were carried out on these relaxed structures using the ANADDB module of the ABINIT package [22, 23], which implements a direct calculation of the strain derivatives of the quantities of interest (Kohn-Sham wavefunctions, polarizations, etc.) via the chain rule. Then, a finite-difference technique was used in order to obtain the non-linear bulk piezoelectric tensors $\widetilde{B}_{\mu jk}$. Specifically, we considered strain states of the form $\eta_1 = \eta_2 = \eta_3 = 0$ and $\eta_4 = \eta_5 = \eta_6 = \gamma$ for several small values of γ. With the strain frozen in for a particular value of γ, the ions were allowed to relax, after which the reduced piezoelectric tensor elements $\tilde{e}_{11}(\gamma)$, $\tilde{e}_{12}(\gamma)$ and $\tilde{e}_{15}(\gamma)$ were computed using linear-response techniques as before. The dependence of these elements on γ was then fitted, and the linear dependence extracted. From Eq. (2), this determines the three independent elements of the $\widetilde{B}$ tensor as $\widetilde{B}_{114} = d\tilde{e}_{11}/d\gamma$, $\widetilde{B}_{124} = d\tilde{e}_{12}/d\gamma$, and $\widetilde{B}_{156} = d\tilde{e}_{15}/d\gamma$. The results for GaAs and InAs are given in Table I.

Calculation of the piezoelectric field for large structures (non self-consistent Poisson approach): The DFT method cannot be applied to 10^3-10^6-atom structures which are often of interest in nanoscience. Instead, such structures can only be calculated by non self-consistent methods (e.g., tight binding, *k.p*, empirical pseudopotentials), in which case piezoelectricity must be added as an external potential. Thus, to model such structures, we first calculate the strain tensor η at each atom site using the valence force field (VFF) method. In this method, the bond-stretching, bond-bending, and mixed bending-stretching terms are derived from experiment. The method has been shown to give accurate atomic positions for defect-free bulk and alloys. For example, Bernard and Zunger compared strain values obtained by LDA and by VFF for the extreme case of a single monolayer InAs superlattice in GaAs and obtaining agreement within 0.4% [24]. From a knowledge of the strain field $\eta_j(\mathbf{r})$, we can use Eq. (1) to obtain $p_\mu(\mathbf{r})$, and the piezoelectric charge density (per unit undeformed volume) is then calculated from the divergence (in undeformed coordinates) of p_μ via

$$\rho_{\rm piezo}(\mathbf{r}) = -\frac{e}{a_0^2}\nabla\cdot\mathbf{p} \quad . \tag{3}$$

The calculation of the divergence [Eq. (3)] is performed using a piecewise polynomial function to represent the polarization data points. Finally, the piezoelectric potential $V_{\rm piezo}$ is obtained from a finite-grid solver of the Poisson equation

$$\rho_{\rm piezo}(\mathbf{r}) = \epsilon_0\nabla\cdot\{\epsilon_s(\mathbf{r})\nabla V_{\rm piezo}(\mathbf{r})\} \quad , \tag{4}$$

where we assume an isotropic local static dielectric constant $\epsilon_s(\mathbf{r})$. However, note that the local polarization cannot be defined on an arbitrarily small region of space[25], but only on a scale that exceeds the localization of the maximally localized Wannier functions [26]. For GaAs and InAs we average the strain tensor over eight-atom clusters. The piezoelectric tensor of Eq. (2) is position dependent since it depends on the inhomogeneous strain. Furthermore, for alloys or heterostructures, $\tilde{e}_{\mu j}(\mathbf{r})$ also depends on the material concentration at $\mathbf{r}$. In our case we have regions in the cell with InAs, GaAs, or mixed (In,Ga)As, and we use a linear interpolation

$$A(\mathbf{r}) = xA_{\rm InAs}(\mathbf{r}) + (1-x)A_{\rm GaAs}(\mathbf{r}) \tag{5}$$

of the tensors ($A = e_{\mu j}$ or $B_{\mu jk}$) between the constituent bulk materials for the given local concentration x of the eight-atom cell. Finally, the solution of the Poisson equation [Eq. (4)] is obtained on the eight-atom-cluster grid through a conjugate-gradient algorithm with a position-dependent dielectric constant $\epsilon_s(\mathbf{r})$ calculated according to Eq. (5) with $A = \epsilon_s$. The approach developed for the calculation of $V_{\rm piezo}$ can be applied easily to very large (10^6-atom) nanostructures.

Testing the non-self-consistent Poisson approach: We tested the non-self-consistent procedure described in Eqs. (1)-(4) by comparing the results with direct self-consistent DFT calculations for a model quantum well of artificially small dimensions which can be handled by DFT. The system is a 30-atom [111] InAs quantum-well

$[(InAs)_6(GaAs)_9]$ epitaxially strained to the GaAs in-plane lattice constant. For the DFT calculations, we used the same pseudopotentials and convergence parameters as in the calculation of the piezoelectric tensors. To obtain the piezoelectric field directly from the DFT-LDA quantum-well calculations, we averaged out the atomic oscillations from the self-consistent Kohn-Sham potential (including ionic, Hartree and LDA exchange-correlation contributions). The direct DFT results of this averaging procedure[27] are denoted in Fig. 1 as the "SCF DFT-LDA" curve. (A linear regression of the obtained curve in the region marked with "Linear Fit" gives a value for the piezoelectric field of 1255 kV/cm.) The piezoelectric potential obtained with the procedure of Eqs. (1)-(4) is given in Fig. 1 as the dashed curve denoted "non-SCF Poisson". The potential jump at the interface is related to the band offset between materials [27] and is not present in the bare piezoelectric potential given by the dashed curve. The potentials are arbitrarily shifted to coincide in the InAs region. We see that the field deduced from the non-SCF procedure is 1367 kV/cm, in very good agreement with the self-consistent DFT-LDA quantum-well result of 1255 kV/cm.

Application to large quantum-well structures. Having established the validity of the non-self-consistent method for small systems, where comparison with DFT-LDA is possible, we now address nanostructures with sizes and composition typical of experimental conditions. We chose here the quantum well system $In_xGa_{1-x}As/GaAs$ where the $In_xGa_{1-x}As$ alloy is epitaxially grown on the GaAs substrate and the thickness of the well is around 10 nm. We use 12,000 atoms in the simulation cell to accurately represent the random alloy. We plot in Fig. 2 the piezoelectric potential (in mV) along the [111] direction for In concentration x=0.1 to 1.0. Figure 2 shows a linear potential along the growth axis, as expected from the fact that the piezoelectric charges are well localized at the interfaces. The small oscillations in the potential are due to random alloy fluctuations which are most prominent at low In concentrations. Interestingly, Fig. 2 shows that the field reverses sign between $x = 0.4$ and 0.3, going from a very strong positive field (i.e., negative slope along [111]) for In-rich wells to a weak negative field in the In-poor regime.

The piezoelectric field extracted from the potential of Fig. 2 is shown in Fig. 3 as a function of the In concentration (circles). Figure 3(b) shows the electric field with an emphasis on the experimentally relevant concentration range from x= 0.10 to 0.25. We see that the amplitude of the field obtained with both linear and nonlinear terms is much smaller than the field obtained with $e_{\mu j}$ only. Considering the full concentration range, the field obtained using both $e_{\mu j}$ and $B_{\mu jk}$ is shown to be negative at low In concentrations and almost constant until it reaches 30%, where it reverses sign and becomes very strong. The field we obtain for a concentration range of 16-20% In is nearly constant around 80 kV/cm.

A direct comparison of calculated and measured electric fields is difficult because only few experiments report the value of the measured field and the measurements and calculations are performed on different concentrations and thicknesses. Cho *et al.*[20] obtained a field of 129 ± 12 kV/cm for a 17 % In well with an estimated 8.7 nm thickness, and Sanchez *et al.* obtained a field of 137 ± 6 kV/cm for a 17% In well with 10 nm thickness and 121 ± 5 kV/cm for a 10 nm thick well with 21% In concentration. Furthermore, the results are clouded by strong temperature effects [17, 20, 21] (pyroelectricity) and possible effects of In segregation [19]. However, one experimental observation that does not seem to depend on well concentration and thickness is the fact that the measured piezoelectric field leads to an e_{14} value that is about 35% smaller than what is expected by using the linear coefficients alone. This has been reported on many occasions [16, 17, 18, 20, 28] and constitutes an unsolved puzzle. This result can be accurately compared with our calculations. If we calculate the piezoelectric field using the experimental value of e_{14} for bulk InAs (-0.045 C/m^2) and bulk GaAs (-0.160 C/m^2) and neglecting the second-order tensors $B_{\mu jk}$ in Eq. (1) (triangular symbols in Fig. 3), which is equivalent to the experimental procedure that leads to an overestimation of e_{14} by 35%, we find for the concentration region of $\simeq$18-21%, an overestimation of the magnitude of the field by 34-52%. Our results therefore explain the origin of the experimentally observed deviation [16, 17, 18, 20, 28] : a linear interpolation between the InAs and GaAs values of e_{14} cannot reproduce the piezoelectric field of alloyed quantum wells since the field does not originate from the linear coefficient alone but has significant contributions from the second-order piezoelectric tensors $B_{\mu jk}$ (neglected in the analysis of the experimental results).

To emphasize the effect of the non-linear tensors $B_{\mu jk}$ further, we plot using square symbols in Fig. 3 the piezoelectric field with $e_{\mu j}$ set to the DFT values and $B_{\mu ij}$ set to zero. The results show that, when taking only the linear tensor into account, the field is overestimated by about 200% in the region of low concentration [Fig. 3(b)], and even has the wrong sign at higher concentrations.

In summary, we have shown that the second-order piezoelectric tensor, generally neglected so far in theoretical and experimental work, contributes significantly to the piezoelectric effect in zincblende semiconductors. We showed that the piezoelectric field calculated by including first- and second-order piezoelectric tensors obtained from DFT agree well with experiments, whereas neglect of non-linearities leads to qualitative disagreements. We argue that the "piezoelectric coefficients" that have been extracted from experimental work so far are actually effective ones reflecting equally strong first- and second-order contributions.

This work has been supported by U.S. DOE-SC-BES-

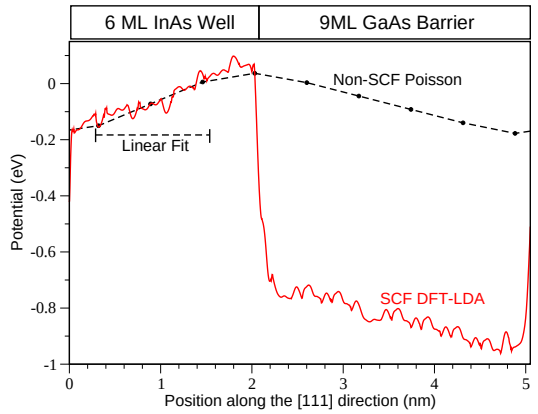


FIG. 1: (Color online) Piezoelectric potential calculated from Eqs. (1) to (4) (dashed line) and the Kohn-Sham potential obtained from self-consistent DFT calculations (solid line). Both calculations are for an $(InAs)_6/(GaAs)_9$ superlattice epitaxially strained on GaAs.

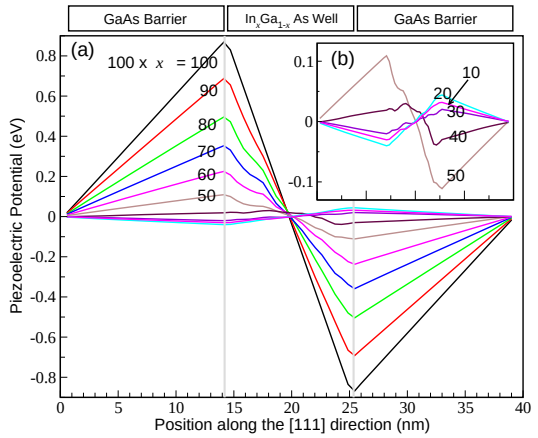


FIG. 2: (Color online) (a) Piezoelectric potential calculated from Eqs. (1-4) for an 11 nm $In_xGa_{1-x}As$ well epitaxially strained to GaAs for $x = 0.1$ - 1.0. (b) for $x = 0.1$ - 0.5.

DMS under LAB 03-17 initiative and by NSF Grant DMR-0233925.

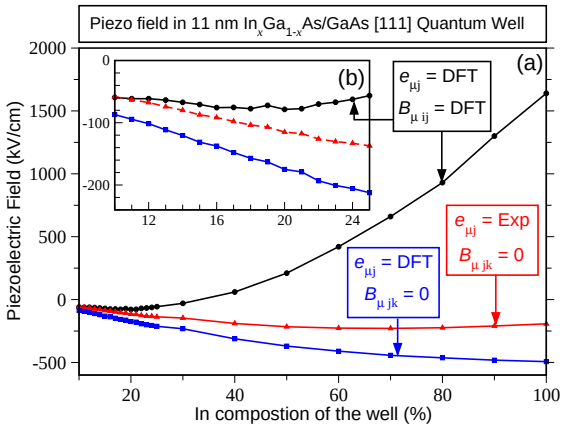


FIG. 3: (Color online) (a) Piezoelectric field as a function of x. Circles: correct result with linear and non-linear piezoelectric tensors from DFT. Triangles: neglecting $B_{\mu jk}$ and using experimental $e_{\mu j}$. Squares: neglecting $B_{\mu jk}$ and using LDA $e_{\mu j}$. (b) Magnification of the low-concentration region.

[1] W. G. Cady, *Piezoelectricity* (McGraw-Hill, New York, 1946).
[2] G. Arlt and P. Quadflieg, Phys. Stat. Sol. **25**, 323 (1968).
[3] R. M. Martin, Phys. Rev. B **5**, 1607 (1972).
[4] K. Hubner, Phys. Stat. Sol. (b) **57**, 627 (1973).
[5] W. A. Harrison, Phys. Rev. B **10**, 767 (1974).
[6] R. D. King-Smith and D. Vanderbilt, Phys. Rev. B **47**, 1651 (1993); D. Vanderbilt, J. Physics and Chemistry of Solids **61**, 147 (2000).
[7] S. deGironcoli, S. Baroni, and R. Resta, Phys. Rev. Lett. **62**, 2853 (1989); A. DalCorso, R. Resta, and S. Baroni, Phys. Rev. B **47**, 16252 (1993); F. Bernardini, V. Fiorentini, and D. Vanderbilt, Phys. Rev. B **56**, R10024 (1997); F. Bernardini and V. Fiorentini, Phys. Rev. B **64**, 085207 (2001).
[8] D. L. Smith and C. Mailhiot, Reviews of Modern Physics **62**, 173 (1990).
[9] O. Stier, M. Grundmann, and D. Bimberg, Phys. Rev. B **59**, 5688 (1999).
[10] A. D. Andreev and E. P. O'Reilly, Phys. Rev. B **62**, 15851 (2000).
[11] M. Holm, M. E. Pistol, and C. Pryor, J. Appl. Phys. **92**, 932 (2002).
[12] W. Sheng and J. P. Leburton, Phys. Rev. B **67** 125308 (2003).
[13] V. Ranjan,et al., Phys. Rev. B **68**, 115305 (2003).
[14] G. Bester and A. Zunger, Phys. Rev. B **71**, 045318 (2005).
[15] R. A. Hogg , et al., Phys. Rev. B **48**, R8491 (1993).
[16] J. L. Sanchez-Rojas,et al., Appl. Phys. Lett. **65**, 2042 (1994).
[17] T. B. Bahder, R. L. Tober, and J. D. Bruno, Phys. Rev. B **50**, R2731 (1994).
[18] P. Ballet, et al., Thin Solid Films **336**, 354 (1998).
[19] P. Ballet,et al., Phys. Rev. B **59**, R5308 (1999).
[20] S. Cho,et al., J. Appl. Phys. **90**, 915 (2001).
[21] J. J. Sanchez,et al., J. Appl. Phys. **91**, 3002 (2002); S. Cho,et al., Phys. Stat. Sol. (a) **195**, 260 (2003).
[22] ABINIT is a common project of the Université Catholique de Louvain, Corning Incorporated, and other contributors (http://www.abinit.org). See X. Gonze, Comp. Mat. Sci **25**, 478 (2002).
[23] X. Wu, D. Vanderbilt, and D.R. Hamann, Phys. Rev. B **72**, 035105 (2005).
[24] J. Bernard and A. Zunger, Appl. Phys. Lett. **65**, 165 (1994).
[25] R. Resta, Rev. Mod. Phys. **66**, 899 (1994).
[26] N. Marzari and D. Vanderbilt, Phys. Rev. B **56**, 12847 (1997).
[27] A. Baldereschi, S. Baroni, and R. Resta, Phys. Rev. Lett. **61**, 734 (1988).
[28] C. H. Chan,et al., Appl. Phys. Lett. **72**, 1208 (1998); S. A. Dickey,et al., Microelectronic Engineering **43-4**, 171 (1998); J. D. Bruno and R. L. Tober, J. Appl. Phys. **85**, 2221 (1999).